Layered T2-, O6-, O2-, and P2-Type $A_{2/3}[M'^{2+}_{1/3}M^{4+}_{2/3}]O_2$ Bronzes, A = Li, Na; M′ = Ni, Mg; M = Mn, Ti

J. M. Paulsen, R. A. Donaberger,† and J. R. Dahn*

Department of Physics, Dalhousie University, Halifax, Nova Scotia B3H 3J5, Canada

Received December 28, 1999. Revised Manuscript Received May 15, 2000

Layered compounds $A_{2/3}[M'^{2+}_{1/3}M^{4+}_{2/3}]O_2$ are studied for A = Li, Na, M′ = Ni, Mg, and M = Mn, Ti. The metastable compounds with A = Li have been uniformly prepared from P2 structure precursors with A = Na by ion exchange. For the cases M′ = Ni, Mg and M = Mn we find that the cations within a $[M'^{2+}_{1/3}M^{4+}_{2/3}]O_2$ sheet are ordered on a $(\sqrt{3})a$ by $(\sqrt{3})a$ superlattice that is preserved during ion exchange. The in-plane ordering is exactly the same as found for the Li and Mn atoms in the layered compound $Li[Li_{1/3}Mn_{2/3}]O_2$, better known as Li_2MnO_3. When M = Ti, no evidence for transition metal ordering is observed. Using the results from X-ray and neutron scattering, $Li_{2/3}[Ni_{1/3}Mn_{2/3}]O_2$ is shown to adopt a new orthorhombic structure that we call T2. In the notation of Hagenmuller and Delmas, the T2 structure has a two-layer unit cell and tetrahedral sites for lithium. $Li_{2/3}[Mg_{1/3}Mn_{2/3}]O_2$ adopts an O6 structure. The focus of the work is the novel T2 structure, and we give crystallographic arguments for the formation of T2 versus O6 based on the detailed stacking of the ordered transition-metal layers.

Introduction

$Li_{2/3}[Ni_{1/3}Mn_{2/3}]O_2$ is a layered Li−transition-metal oxide, which has an O2-type structure.[1] It exhibits a large reversible capacity of 180 mA h/g in $Li/Li_{2/3}[Ni_{1/3}Mn_{2/3}]O_2$ electrochemical cells and can be cycled at room temperature or 55 °C with very high capacity retention. The material is synthesized by ion-exchanging the sodium in $P2\text{-}Na_{2/3}[Ni_{1/3}Mn_{2/3}]O_2$ for lithium. Immediately after ion-exchange, $Li_{2/3}[Ni_{1/3}Mn_{2/3}]O_2$ has an unknown structure that is apparently related to the O2 structure. This transforms to the ideal O2 structure when lithium is added or removed from the compound by electrochemical intercalation.[1] Then, the O2 structure remains stable during cycling and does not convert back to the original unknown structure. The explanation of the unknown initial structure is one aim of the present work.

Ion-exchange reactions in layered bronzes were investigated by Hagenmuller and Delmas more than 10 years ago,[2−4] and they developed a convenient structural nomenclature, which we adopt here. They classified the structure of layered A_xMO_2 bronzes into groups (P2, O2, O6, P3, O3), which allows an understanding of ion-exchange reactions.[4,5] The letter indicates the site of the alkali metal, A (prismatic or octahedral), and the number gives the number of MO_2 sheets (M = transition metal) in the unit cell. The transition metal is located in octahedral sites between two oxygen layers, making a MO_2 sheet. The MO_2 sheets are separated by the alkali metals. The structure types differ by the arrangement of neighboring MO_2 sheets.

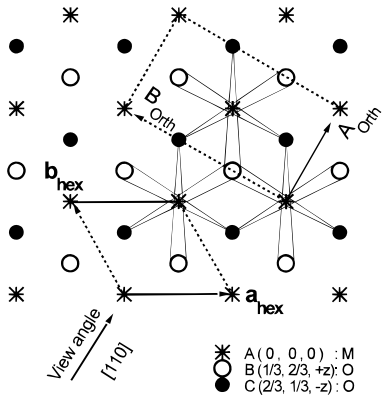

Figure 1. A MO_2 (transition-metal−oxygen layer) displayed in hexagonal stacking, viewed down the [001] direction. The bases of the natural unit cells are given. The rhombus is the base of the "small hexagonal" cell, and the rectangle is the base of the "small orthorhombic" or "small monoclinic" unit cell. Viewing the MO_2 layer from the [110] direction is especially suited to describe hexagonal stacking sequences. (This view makes rows of atoms for each type.)

Figure 1 shows the stacking of one MO_2 sheet, seen from the [001] direction. If the various structures are viewed along the [110] direction, then the oxygen and transition-metal atoms are aligned in rows and the structures are particularly easy to display. Different stacking sequences and orientations of the MO_2 sheets lead to the different structures, some of which are shown in [110] projections given in Figure 2. The alkali metals are not shown in Figure 2 for clarity. Notice that the

† Steacie Institute of Molecular Sciences, National Research Council of Canada, Ottawa, Ontario, Canada.

(1) Paulsen, J. M.; Thomas, C. L.; Dahn, J. R.; *J. Electrochem. Soc.* **2000**, *147*, 861.
(2) Delmas, C.; Braconnier, J.-J.; Maazaz, A.; Hagenmuller, P. *Rev. Chim. Miner.* **1982**, *19*, 343.
(3) Delmas, C.; Braconnier, J.-J.; Hagenmuller, P. *Mater. Res. Bull.* **1982**, *17*, 117.
(4) Mendiboure, A.; Delmas, C.; Hagenmuller, P. *Mater. Res. Bull.* **1984**, *19*, 1383.
(5) Delmas, C.; Fouassier, C.; Hagenmueller, P. *Physica* **1980**, *99B*, 81.

10.1021/cm990810d CCC: $19.00
Published on Web 07/11/2000

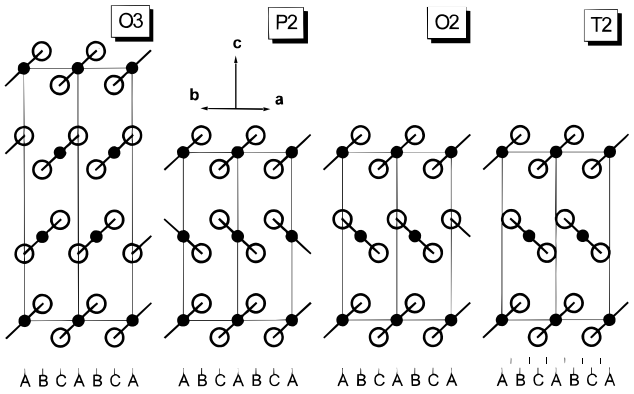

Figure 2. Layered structures consisting of rigid MO_2 sheets viewed from the [110] direction.

O3 and P3 (not shown) structures differ from the P2, O2, and O6 (not shown) structures, in that all the MO_2 layers in the former group have the same orientation, while those in the latter group do not. Low-temperature ion-exchange reactions allow transformations within a structural group by layer gliding, but not between them. For example, O2-$LiCoO_2$ has been prepared from P2-Na_xCoO_2 (2) whereas O3-$LiCoO_2$ can be prepared from P3-$NaCoO_2$ by ion exchange. We want to focus on the group containing the P2, O2, and O6 structures since the precursor P2-$Na_{2/3}[Ni_{1/3}Mn_{2/3}]O_2$ and the novel cathode material $Li_{2/3}[Ni_{1/3}Mn_{2/3}]O_2$ prepared from this precursor belong to this group. Typical for this group are unit cells with two MO_2 sheets. [The O2 and P2 structures have two sheets in the unit cell. The O6 structure has six MO_2 layers using the rhombohedral space group *R*-3*m*. However, if a monoclinic unit cell of lower symmetry is used, then the O6 structure can be described with only two MO_2 layers per unit cell.]

The materials described in this work differ from those studied previously, in that two different cations, M′ and M, in a 1/3:2/3 stoichiometric ratio make the transition-metal layer in the $A_x[M'_{1/3}M_{2/3}]O_2$ structure. Therefore, we expect that an ordering of M′ and M, producing a $(\sqrt{3})a$ by $(\sqrt{3})a$ superlattice, may occur. The well-known Li_2MnO_3, better written as $Li[Li_{1/3}Mn_{2/3}]O_2$, is the prototypical layered bronze that displays ordering on the $(\sqrt{3})a$ by $(\sqrt{3})a$ a superlattice in the metal atom plane that contains 1/3 Li and 2/3 Mn atoms. However, $Li[Li_{1/3}Mn_{2/3}]O_2$ has the O3 structure, not belonging to the group of two layer unit cells.

The structure of $Li_{2/3}[Ni_{1/3}Mn_{2/3}]O_2$ does not adopt any of the previously described structures. Instead, it has a new structure that we call T2 as shown in Figure 2. The T2 structure is achieved by a gliding of rigid MO_2 layers, but it has tetrahedral (hence T), not octahedral, sites for the lithium. An integral part of the T2 structure is a $(\sqrt{3})a$ by $(\sqrt{3})a$ superlattice ordering of the cations in the metal layer. Without the cation ordering, the T2 structure would not form. Whereas O2, P2, and O6 are hexagonal or rhombohedral structures, the new T2 structure is orthorhombic. The oxygen stacking in the T2 structure cannot be given in a hexagonal stacking. In principle, the T2 structure is not limited to $Li_{2/3}[Ni_{1/3}Mn_{2/3}]O_2$, and it should be added to the list of structures that can be obtained by ion-exchanging P2 sodium bronzes.

Organization of This Paper

Single crystals of the phases investigated in this work could not be prepared, so a complete proof of their structures is not easy. The powder diffraction patterns are complicated since the cation ordering is not perfect. Additionally, stacking faults are observed. These problems will be sketched in the section Structural Prerequisites. Here, different unit cells necessary to understand the structures will be defined. Then, as an example of such complicated powder diffraction patterns, the well-known $Li[Li_{1/3}Mn_{2/3}]O_2$ will be discussed.

In the Structure of $Li_{2/3}[Ni_{1/3}Mn_{2/3}]O_2$: X-ray Investigation, high-resolution X-ray diffraction of crystalline powders shows that the structure of the investigated $Li_{2/3}[Ni_{1/3}Mn_{2/3}]O_2$ cannot be described by conventional hexagonal or rhombohedral space groups. A novel, orthorhombic structure (T2 structure) will be suggested. An unconventional Rietveld refinement had to be made since the powder diffraction pattern exhibits irregularities. Li is almost "invisible" by X-ray, and Ni and Mn have similar scattering powers, making them almost indistinguishable, so the solution of the structure from X-ray data alone is difficult. Therefore, the proposed structure had to be proved by neutron diffraction, where Ni, Mn, and Li are distinguishable, which is done in the section Confirmation of the Transition-Metal Ordering in T2-$Li_{2/3}[Ni_{1/3}Mn_{2/3}]O_2$ by Neutron Diffraction.

The section Structure of O6-$Li_{2/3}[Mg_{1/3}Mn_{2/3}]O_2$ investigates a $Li_{2/3}MO_2$ phase which instead of Ni contains Mg. The X-ray diffraction shows that $Li_{2/3}[Mg_{1/3}Mn_{2/3}]O_2$ has a $(\sqrt{3})a$ by $(\sqrt{3})a$ cation ordering as well, but it does not exhibit the T2 structure. Instead it crystallizes in the O6 structure. We assumed that the different structure is caused by a different cation ordering in the precursor P2 phases. Therefore, in the sections Structure of the Precursor $Na_{2/3}[Ni_{1/3}Mn_{2/3}]O_2$ and Structure of the Precursor $Na_{2/3}[Mg_{1/3}Mn_{2/3}]O_2$, the structures of the sodium precursors $Na_{2/3}[Ni_{1/3}Mn_{2/3}]O_2$ and $Na_{2/3}[Mg_{1/3}Mn_{2/3}]O_2$ are investigated by X-ray and neutron diffraction. We show that $Na_{2/3}[Ni_{1/3}Mn_{2/3}]O_2$ has a hexagonal P2 structure with an $A_2A_3A_2A_3$ stacking of ordered Ni−Mn layers. Contrary to this, $Na_{2/3}[Mg_{1/3}Mn_{2/3}]O_2$ has the alternative $A_1A_1A_1A_1$ stacking of ordered Mg−Mn layers.

In the Discussion it will be argued that only the $A_2A_3A_2A_3$-ordered P2 precursors can give the T2 structure (as is the case for P2-$Na_{2/3}[Ni_{1/3}Mn_{2/3}]O_2 \Rightarrow$ T2-$Li_{2/3}[Ni_{1/3}Mn_{2/3}]O_2$), whereas $A_1A_1A_1A_1$-ordered P2 precursors will lead to monoclinic phases as evident for P2-$Na_{2/3}[Mg_{1/3}Mn_{2/3}]O_2 \Rightarrow$ O6-$Li_{2/3}[Mg_{1/3}Mn_{2/3}]O_2$. Additionally, results for $Na_{2/3}[Ni_{1/3}Ti_{2/3}]O_2$ and the ion-exchanged $Li_{2/3}[Ni_{1/3}Ti_{2/3}]O_2$ are given in the section P2-$Na_{2/3}[Ni_{1/3}Ti_{2/3}]O_2$ and O2-Type $Li_{2/3}[Ni_{1/3}Ti_{2/3}]O_2$. Here no evidence for cation ordering appears.

Experimental Section

Preparation. Table 1 gives an overview of the $Li_{2/3}MO_2$ samples and $Na_{2/3}MO_2$ precursors. A crystalline sample (LiNi1) of T2-$Li_{2/3}[Ni_{1/3}Mn_{2/3}]O_2$ was prepared by ion exchange from a crystalline P2-$Na_{2/3}[Ni_{1/3}Mn_{2/3}]O_2$ precursor (NaNi1). The precursor NaNi1 was prepared by solid-state reaction for more than two weeks using manganese and nickel acetate sources. The

Table 1. Sample Preparation

(a) Na-Containing Precursors

precursor		first calcination	second calcination	remarks	cation ordering
NaNi1	nickel and manganese acetate, Na_2CO_3	>2 weeks, 900−1000 °C		excess Na	$A_2A_3A_2A_3$
NaMg1	$(MgCO_3)_4Mg(OH)_2{\cdot}5H_2O$, $MnCO_3$, Na_2CO_3	1 day, 900 °C, air	2 day, 800 °C, air	$Na_{2/3}[Mg_{0.2}Mn_{0.8}]O_2$	$A_1A_1A_1A_1$
NaMg2				$Na_{2/3}[Mg_{1/4}Mn_{3/4}]O_2$	
NaMg3				$Na_{2/3}[Mg_{0.3}Mn_{0.7}]O_2$	
NaTi	$Ni(OH)_2$, TiO_2 (anatase), Na_2CO_3	1 day, 1000 °C, air	1 day, 1000 °C, air	$Na_{2/3}[Ti_{1/3}Mn_{2/3}]O_2$	not detected

(b) Li-Containing Samples

sample	precursor	ion exchange[a]	composition	structure
LiNi1	NaNi1	MS, 280 °C, 5 h, repeated	$Li_{2/3}[Ni_{1/3}Mn_{2/3}]O_2$	T2
LiMg2	NaMg2	MS, 330 °C, 15 h	$Li_{2/3}[Mg_{1/4}Mn_{3/4}]O_2$	O6
LiMg3	NaMg3	MS, 330 °C, 15 h	$Li_{2/3}[Mg_{0.3}Mn_{0.7}]O_2$	
LiTi	NaTi	LiCl + LiOH in H_2O, 15 h, room temperature	$Li_{2/3}[Ni_{1/3}Ti_{2/3}]O_2$	O2 type

[a] MS = molten salt.

temperature was $T = 1000$ °C. An excess ($x > 2/3$) of sodium was used (nominal composition approximately $Na_{0.75}Ni_{1/3}Mn_{2/3}$). The excess sodium makes a highly soluble dark-green phase that can be easily washed away in water. The crystallites reached a size of up to 20 μm. However, single crystals of sufficient quality suitable for single-crystal X-ray diffraction were not obtained. Sample LiNi1 was prepared by ion exchange of precursor NaNi1 in molten salt ($LiNO_3$ + LiCl eutectic) for 5 h at 280 °C.[1]

For comparison, a series of $Li_{2/3}[Mg_xMn_{1-x}]O_2$ samples ($x = 0.2$, 0.25, 0.3, 0.33) were prepared from the P2 structure precursors, $Na_{2/3}[Mg_xMn_{1-x}]O_2$. The P2 precursors $Na_{2/3}[Mg_xMn_{1-x}]O_2$ were prepared by a repeated solid-state reaction. Powders of stoichiometric amounts of $(MgCO_3)_4Mg(OH)_2{\cdot}5H_2O$, Na_2CO_3, and $MnCO_3$, were reacted at 900 °C in air for 1 day. After grinding, pellets were pressed again and were tempered for another 2 days at 800 °C. Alternatively, Na precursors were tempered at 1000 °C for 1 day. Some results for $Na_{2/3}[Mg_xMn_{1-x}]O_2$ will be given here. It seems that the theoretical doping limit of $x = 1/3$ (when Mn reaches its limiting valence state of 4+) cannot be achieved. The limiting Mg-doping level increased from approximately $x = 0.25$ at 1000 °C to $x = 0.3$ at 800 °C. [This is caused by the tendency of Mn to adopt a lower oxidation state as the temperature is increased.] Larger values of x lead to the coexistence of MgO with $Na_{2/3}[Mg_xMn_{1-x}]O_2$. The color of the precursors was dark brown for $x = 0.2$ and changed to bright red-brown, almost red for $x = 0.3$. The ion exchange was made in molten salt at 330 °C for 12 h. The precursor $x = 0.25$ and $x = 0.3$ tempered at 800 °C ion-exchanged well. This work will investigate the sample LiMg3 ($x = 0.3$) and the precursors NaMg1, NaMg2, and NaMg3 ($x = 0.2$, $x = 0.25$ and $x = 0.3$) tempered at 800 °C.

Sample LiTi with composition $Li_{2/3}[Ni_{1/3}Ti_{2/3}]O_2$ was prepared from precursor NaTi with composition $Na_{2/3}[Ni_{1/3}Ti_{2/3}]O_2$. Precursor NaTi was prepared by a repeated solid-state reaction (two heatings for 1 day each at 1000 °C in air) from stoichiometric amounts of TiO_2 (anatase), $Ni(OH)_2$, and Na_2CO_3. Sample LiTi was prepared by adding $Na_{2/3}[Ni_{1/3}Ti_{2/3}]O_2$ to a 2 M (in Li^+) solution containing 1/2 LiOH and 1/2 LiCl. A large excess of lithium (Li:Na approximately 10:1) was used. The ion exchange was made for 15 h at room temperature. Ion exchange at higher temperatures using molten salt is less successful. (We observed a rapid collapse of the layered structure of O2-$Li_{2/3}[Ni_{1/3}Ti_{2/3}]O_2$.)

X-ray and Neutron Diffraction. X-ray diffraction was made using Siemens D500 and D5000 machines equipped with Cu target X-ray tubes and diffracted beam monochromators. For high-resolution measurements, the D5000 diffractometer, long counting times (20 s/0.02° step), and narrow slits were used (0.3° angular divergence). To reduce the preferred orientation, Super S carbon black (MMM Carbon, Belgium) was added to some samples (approximately 2 wt %). This small amount of carbon contributes a small additional background almost undetectable in the diffraction pattern, but helps to maintain random orientation of powder grains. Alternatively, powders were sieved, and the fraction with $180 > d > 45$ μm (d = particle size) was used. In this size range, particles are aggregates of randomly orientated crystallites that do not tend to show preferred orientation. Profile refinement of the collected data was made using Hill and Howard's version of the Rietveld program.[6]

Neutron diffraction measurements were performed using the DualSpec powder diffractometer at AECL Chalk River. Approximately 5 g samples were packed into 5 mm inside diameter thin-walled vanadium cans and measured between scattering angles of 5° and 117° using a wavelength of 1.3276 Å. The samples were continuously rotated during the measurement. Rietveld refinements, using Hill and Howard's program, were made on the original data and are displayed in Figures 12 and 13 with unaltered scattering angles.

Structural Prerequisites

Different unit cells are useful to describe stacking in layered bronzes. Figure 2 shows unit cells which will be called small hexagonal cells. These unit cells describe the structural group (i.e., O2, P2, O6, O3, P3). They do not describe the cationic superstructure ordering. The natural unit cells in the case of a weak distortion are the small monoclinic or small orthorhombic unit cells.

(6) Hill, R. J.; Howard, C. J. *J. Appl. Crystallogr.* **1985**, *18*, 173. Wiles, D. B.; Young, R. A. *J. Appl. Crystallogr.* **1981**, *14*, 149.

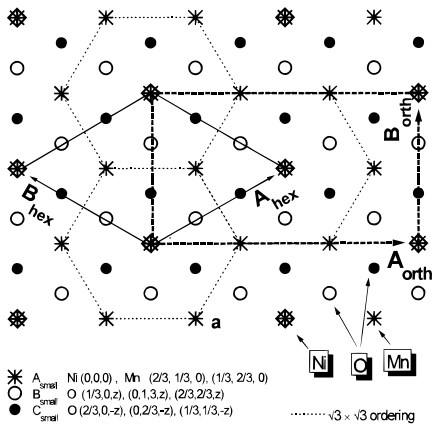

Figure 3. Cation ordering on the $(\sqrt{3})a$ by $(\sqrt{3})a$ superlattice in a MO_2 sheet. Filled and open circles are the oxygen above and below the transition metal. The transition metals nickel and manganese are designated by Ni (asterisk inside square) and Mn (asterisk). The natural unit cell to describe the $(\sqrt{3})a$ by $(\sqrt{3})a$ ordering in MO_2 layers is the "large hexagonal" unit cell and its "large orthorhombic" or "large monoclinic" superstructures. The rhombus (solid line) and rectangle (thick dotted line) give the bases of the large cells.

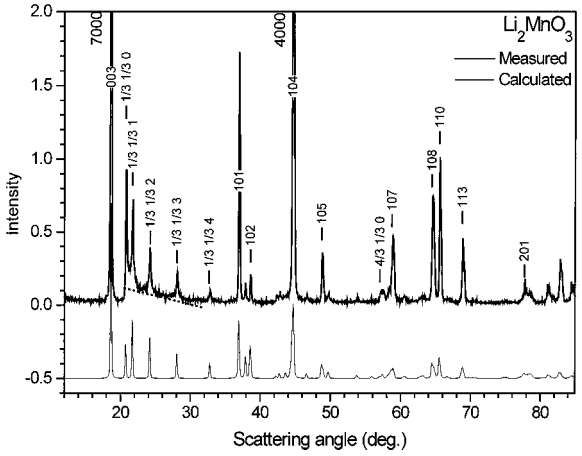

Figure 4. Measured and calculated X-ray diffraction patterns of Li_2MnO_3 as indicated in the legend.

Figure 1 shows the base of a small hexagonal unit cell (the rhombus) as well as the base of a small monoclinic or orthorhombic unit cell (the rectangle). The small hexagonal unit cell has lattice constant $a_{hex} \approx 2.8$ Å, and the small orthorhombic unit cell has lattice constants $a = a_{hex}$ and $b = (\sqrt{3})a_{hex} \approx 5$ Å. In the small monoclinic cell (monoclinic angle defined as β), a_{mon} and b_{mon} have these values too.

Larger unit cells are needed to describe the stacking of the $(\sqrt{3})a$ by $(\sqrt{3})a$ superstructure-ordered MO_2 sheets. Figure 3 displays the superstructure in a single MO_2 sheet with $M = Ni_{1/3}Mn_{2/3}$. The natural unit cell of the $(\sqrt{3})a$ by $(\sqrt{3})a$ superstructure is the large hexagonal cell which has an a axis, A_{hex}, that is $\sqrt{3}$ times larger than that of the small hexagonal unit cell, $A_{hex} \approx 5$ Å. The corresponding large orthorhombic unit cell has $A_{orth} = (\sqrt{3})A_{hex} \approx 8.4$ Å and $B_{orth} = A_{hex} \approx 5$ Å. In the large monoclinic cell, A_{mon} and B_{mon} have these values too.

The diffraction pattern of Li_2MnO_3 is shown in Figure 4. The structure is very close to that of the O3 structure if the superstructure is neglected. However, the ordering is not compatible with any rhombohedral or hexagonal space group, so the unit cell is actually monoclinic. The calculated spectrum used the crystal data of ref 7. The major peaks are indexed using a small hexagonal (rhombohedral) cell in the space group of the O3 structure, $R\text{-}3m$. The peaks (1/3, 1/3, l) are the superstructure peaks due to the Mn−Li ordering, and such peaks are expected when in-plane ordering occurs. This series of peaks have a peculiar shape and a strong sloping background (dotted line in the figure). A satisfying Rietveld refinement of this spectrum using standard software is not possible. The observed intensity ratios of these peaks differ significantly from those of the calculated spectrum. Stacking faults in the arrangement of the ordered layers cause these effects. Stacking faults occur since the coupling between the ordering in neighboring MO_2 layers is not strong.

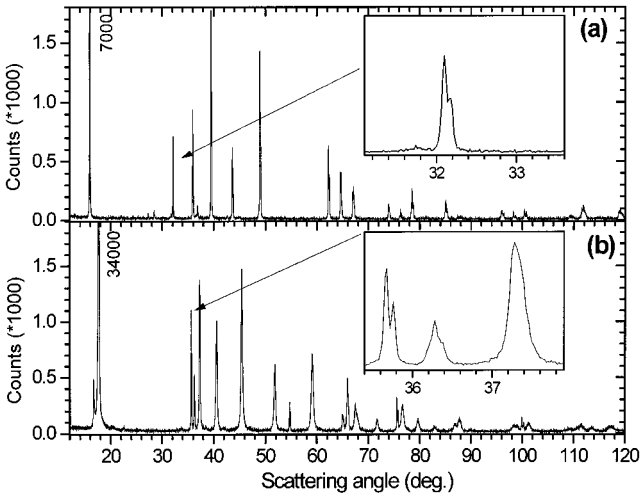

Figure 5. X-ray diffraction pattern of the crystalline bronzes: (a) $Na_{2/3}[Ni_{1/3}Mn_{2/3}]O_2$; (b) $Li_{2/3}[Ni_{1/3}Mn_{2/3}]O_2$. The inset displays the high-resolution (sharp) peaks. Even at 32.1° (a) and 35.7° (b) the $K\alpha_2$ satellite is separated. The inset in panel b shows the anomalous peak widths for $Li_{2/3}[Ni_{1/3}Mn_{2/3}]O_2$. The (0, 0, 4) peak at 35.7° is much sharper than the (1, 0, 0) and (1, 0, 1) peaks at 36.3° and 37.3°. (Miller indices for the small hexagonal unit cell were used.)

Results and Discussion

Structure of $Li_{2/3}[Ni_{1/3}Mn_{2/3}]O_2$: X-ray Investigation. Figure 5a shows the X-ray diffraction pattern of highly crystalline P2-$Na_{2/3}[Ni_{1/3}Mn_{2/3}]O_2$ (precursor NaNi1), and Figure 5b shows the pattern of $Li_{2/3}[Ni_{1/3}Mn_{2/3}]O_2$ (sample LiNi1). The patterns were collected with narrow slits and long counting times to obtain high resolution. The insets show that the crystallinity of both samples and the resolution of the measurement are sufficient to distinguish the $K\alpha_1$ and $K\alpha_2$ peaks even at angles as small as 32°.

The spectrum of $Li_{2/3}[Ni_{1/3}Mn_{2/3}]O_2$ indicates that the ion exchange is almost complete. No peaks of the initial phase remain. The small peak at 16.7° is the remnant of the main peak of an intermediate layered phase with alternating Li and Na layers and a composition of approximately $Li_{1/3}Na_{1/3}[Ni_{1/3}Mn_{2/3}]O_2$ that forms during the ion-exchange reaction.[8]

(7) Brühne, B.; Jansen, M. *Anorg. Allg. Chem.* **1994**, *620*, 1409.
(8) Paulsen, J. M.; Larcher, D.; Dahn, J. R. *J. Electrochem. Soc.*, in press.
(9) Paulsen, J. M.; Dahn, J. R. *J. Electrochem. Soc.*, in press.

Table 2. Observed and Calculated Bragg Peak Positions for the Crystalline Sample LiNi1[a]

peaks observed			hexagonal system $a_{hex} = 2.865 \pm 0.001$ Å $c_{hex} = 10.061 \pm 0.005$ Å					orthorhombic system $a_{orth} = 2.869(4)$ Å $b_{orth} = 4.951(3)$ Å $c_{orth} = 10.063(2)$ Å					
position (deg)	corrected (deg)	fwhm (deg)	*h*	*k*	*l*	calcd (deg)	diff (deg)	*h*	*k*	*l*	calcd (deg)	diff (deg)	wtd diff (deg)
17.613	17.579	0.028	0	0	2	17.617	−0.038	0	0	2	17.612	−0.033	
35.671	35.639	0.050	0	0	4	35.669	−0.031	0	0	4	35.658	−0.019	
36.268	36.235	0.112	1	0	0	36.179	**0.057**	0	2	0	36.256	−0.021	
37.279	37.247	0.139	1	0	1	37.302	−0.055	1	1	1	37.274	−0.027	−0.028
								0	2	1	37.376	−0.160	
40.561	40.528	0.22	1	0	2	40.511	0.017	1	1	2	40.483	0.045	−0.02
								0	2	2	40.579	−0.050	
45.425	45.393	0.24	1	0	3	45.44	−0.047	1	1	3	45.412	−0.019	
51.775	51.744	0.27	1	0	4	51.715	0.030	0	2	4	51.765	−0.020	
54.698	54.667	0.072	0	0	6	54.697	−0.030	0	0	6	54.68	−0.012	
59.054	59.024	0.32	1	0	5	59.066	−0.041	1	1	5	59.035	−0.010	
64.962	64.933	0.31	1	1	0	65.068	**−0.134**	2	0	0	64.945	−0.011	
65.897	65.868	0.21	1	1	1	65.806	0.062	1	3	1	65.888	−0.020	
67.411	67.382	0.38	1	0	6	67.352	0.031	0	2	6	67.385	−0.003	
67.869	67.84	0.31	1	1	2	67.998	**−0.157**	2	0	2	67.875	−0.035	
71.669	71.641	0.30	1	1	3	71.578	0.063	1	3	3	71.653	−0.012	
75.544	75.517	0.096	0	0	8	75.547	−0.030	0	0	8	75.52	−0.003	
76.56	76.533	0.52	1	1	4	76.471	0.062	2	0	4	76.349		
			1	0	7	76.544	−0.012	1	1	7	76.509	0.023	
79.534	79.507	0.46	2	0	2	79.524	−0.016	2	2	2	79.455	0.052	0.03
								0	4	2	79.708	−0.201	
82.793	82.767	0.78	1	1	5	82.622	**0.146**	1	3	5	82.687	0.080	

[a] An indexing is only approximately successful assuming a hexagonal space group. Successful indexing requires the orthorhombic system. The Bragg peak positions were corrected for an off-axis shift of 55 μm. Differences between observed (and corrected) and calculated Bragg peak positions are given. Differences (for the hexagonal system) given in bold font are unacceptably large. The column "wtd Diff " (weighted difference) gives the difference corrected for overlapping peaks.

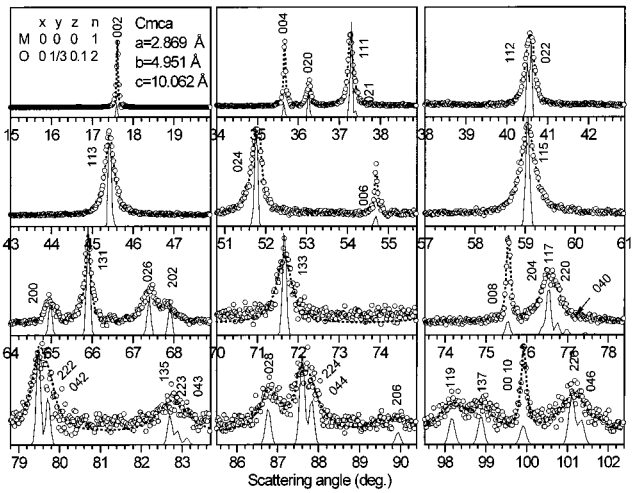

Figure 6. X-ray diffraction pattern of the crystalline $Li_{2/3}[Ni_{1/3}Mn_{2/3}]O_2$. The data are corrected for the $K\alpha_2$ radiation. The solid line gives the peak positions and approximate intensity ratios for a small orthorhombic unit cell (crystal data given in the figure). The observed spectrum is perfectly indexed using this small orthorhombic unit cell. The thick dotted line is a fit of the observed spectrum by Lorentz functions.

Figure 6 shows details of the diffraction pattern of the ion-exchanged $Li_{2/3}[Ni_{1/3}Mn_{2/3}]O_2$ sample LiNi1 corrected for $K\alpha_2$. (The "subtract $K\alpha_2$" routine of the EVA program supplied with the Siemens D500 was used for the subtraction.) Indexing the pattern using a hexagonal unit cell is approximately possible but inaccurate as shown in Table 2. Any choice of hexagonal unit cell leads to small (on the order of 0.1°) systematic differences between the calculated and observed peak positions. The deviations are not of instrumental origin. However, the peaks could be indexed using a (small) orthorhombic unit cell, which allowed the determination of the orthorhombic lattice constants using a least-squares routine. If the transition metals cannot be distinguished, then this small orthorhombic cell can be used to describe the structure. The inset in Figure 6 gives the crystal data, which were used to calculate a diffraction pattern that is shown in the figure by the thin line. It reproduces well the integrated intensities and peak positions of the experimental pattern.

The pattern displayed in Figures 5b and 6 is complex because it shows peak widths that do not vary smoothly as a function of the scattering angle. Because of this, the pattern cannot be simulated with our Rietveld program. To overcome this problem, we fitted the experimental peaks in Figure 6 with Lorentzian peaks, as shown by the dotted lines in the figure. The solid lines in Figure 6 give the positions of the fitted peaks. The intensities and positions of the fitted peaks were then used to generate an intermediate "experimental" pattern with broader but constant peak widths, shown in Figure 7. Rietveld refinement was applied to the intermediate experimental pattern, and the calculated pattern (described below) is the solid line in Figure 7. Since there is no statistical noise in the intermediate experimental pattern, the goodness of fit (equal to the quantity χ^2) returned by the program is less than 1 and could, in principle, reach 0 if the fit were perfect. On the other hand, the Bragg *R* factor ($R_B = 100\sum|I_{measd} - I_{calcd}|/I_{measd}$) is unaffected by the absence of statistical noise. In the refinement the small orthorhombic unit cell with space group *Cmca* was used. A refinement using the large orthorhombic unit cell, i.e., including the cationic superstructure, does not bring any significant improvement, has more free parameters, and is less stable.

The agreement between the experimental and calculated patterns is very good. Attempted refinements using the O2 structure were unacceptable. The refined

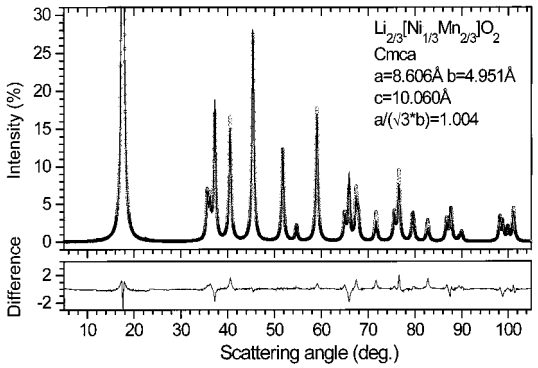

Figure 7. X-ray Rietveld refinement of the intermediate experimental pattern of crystalline $Li_{2/3}[Ni_{1/3}Mn_{2/3}]O_2$ (see the text). Refined crystal data are given in Table 3.

Table 3. Crystal Data of T2-$Li_{2/3}[Ni_{1/3}Mn_{2/3}]O_2$ and P2-$Na_{2/3}[Ni_{1/3}Mn_{2/3}]O_2$ Obtained by X-ray Diffraction of the Crystalline Precursor NaNi1 and Sample LiNi1

T2-$Li_{2/3}[Ni_{1/3}Mn_{2/3}]O_2$[a] space group *Cmca*, orthorhombic					P2−$Na_{2/3}[Ni_{1/3}Mn_{2/3}]O_2$[b] space group $P6_3/mmc$, hexagonal				
$N = 4$	x	y	z	occ	$N = 2$	x	y	z	occ
Ni	0	0		1	$Ni_{1/3}Mn_{2/3}$	0	0	0	1
Mn	1/3	0	0	2	O	2/3	1/3	0.094	1.95
O(1)	0	1/3	0.103	2	Na(1)	0	0	1/4	0.23
O(2)	1/3	1/3	0.109	4	Na(2)	2/3	1/3	1/4	0.35
Li	1/4	1/12	1/4	2					

[a] GOF = 0.9, R_B = 4.65%, A_{orth} = 8.605 Å, B_{orth} = 4.951 Å, C_{orth} = 10.060 Å. [b] GOF = 2.08, R_B = 5.42%, a_{hex} = 2.885 Å, c_{hex} = 11.155 Å.

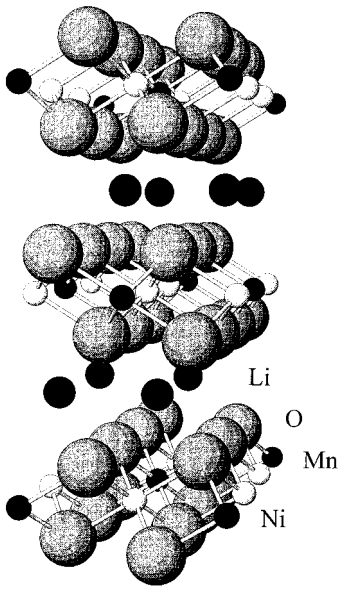

Figure 8. Structure of T2-$Li_{2/3}[Ni_{1/3}Mn_{2/3}]O_2$ (crystal data of Table 3 were used).

crystal data for the T2 structure are given in Table 3. To be consistent with the neutron scattering results (here the cationic superstructure is visible and the large cell is needed), we have converted the crystallographic data to the large orthorhombic cell (see Figure 8) with similar oxygen and transition-metal positions.

The X-ray powder diffraction is not able to distinguish Ni and Mn well since they have almost the same scattering power. In addition, lithium is a very weak scatterer, almost invisible by X-ray diffraction when heavy elements are present. Therefore, the lithium positions as well as the Ni−Mn ordering given in Table 3 and displayed in Figure 8 are hypothetical and have to be confirmed by neutron diffraction. However, the good agreement in Figure 7 suggests that the transition-metal and oxygen positions have been chosen correctly.

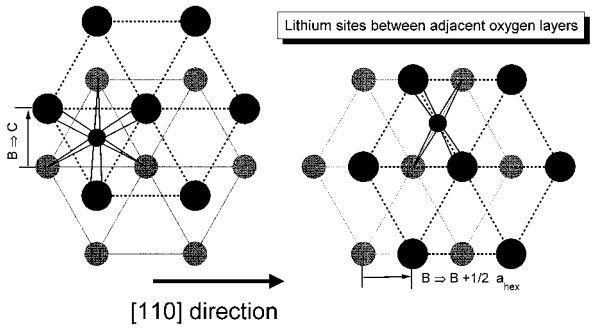

Figure 9. Lithium sites in layered Li_xMO_2 obtained by ion-exchanging a P2-Na_xMO_2 viewed along [001]. The gray circles show the upper oxygen sheet of the lower MO_2 layer. The black circles give the lower oxygen sheet of the upper MO_2 layer. In the starting P2 phase, the oxygen atoms of the two oxygen sheets have the same (x, y) positions. The alkali metals (small black circles) are sandwiched between the two oxygen sheets. Left: Gliding by one hexagonal position yields the O2 structure with lithium in octahedral sites. Right: Gliding by half of a hexagonal lattice vector yields the T2 structure with lithium in distorted tetrahedral sites.

As shown in Figure 2, the transition metals and oxygen atoms in the P2, O2, and T2 structures make MO_2 layers with alternating orientation of adjacent layers. To shift from P2 to O2 during ion exchange, the transition metals in the intermediate layer glide from A to B (Figure 2) perpendicular to the [110] direction of the small hexagonal cell. To transform from P2 to T2, the gliding is different. If the transition metal on the first layer sits on an "A" site, then those of the next layer are located between B and C sites (Figure 2). Figure 9 shows the gliding and the sites for lithium between two adjacent MO_2 layers viewed from the [001] direction. Displayed are the two oxygen layers "above" and "below" the lithium layer. In the original P2 structure these oxygen positions are B sites (Figure 2). The O2 structure is achieved by gliding of the upper layer (large black symbols) from B to C. This gliding makes an octahedral site for lithium. The T2 structure is achieved after gliding of the upper layer by a smaller distance that is half the small hexagonal lattice constant as shown in the right part of Figure 9. Octahedral sites for lithium are not formed. Most likely, lithium is located in the distorted *tetrahedral* site displayed in the figure. Therefore, we call the structure of $Li_{2/3}[Ni_{1/3}Mn_{2/3}]O_2$ T2, T for the tetrahedral sites lithium occupies, and 2 for the two-layer unit cell. Figure 9 shows that the tetrahedral sites for lithium are distorted. All four nearest-neighbor distances are the same, but the angles of the tetrahedra differ from an undistorted tetrahedron. [Viewed from the [001] direction, the four oxygen neighbors make a rectangle. An undistorted tetrahedral site would show the four neighbors as a square.] From the suggested crystal data of Table 3, the following data can be derived: all lithium−oxygen distances are 2.00 Å, and the distorted tetrahedral angles are 90.9°, 103.9°, and 138.1°.

There are a number of compounds that have lithium atoms in distorted tetrahedral sites. For example, in $LiAlSiO_4$ glass, lithium is located in oxygen tetrahedra

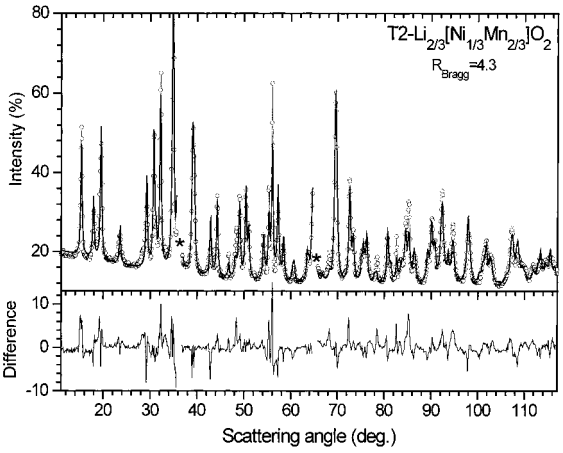

Figure 10. Neutron diffraction data and Rietveld refinement of the T2-$Li_{2/3}[Ni_{1/3}Mn_{2/3}]O_2$ sample LiNi1. Crystal data are given in Table 4. Two regions (containing vanadium peaks originating from the sample holder) marked by asterisks were excluded in the refinement.

with three short bonds (2.02 Å) and one longer bond (2.32 Å).[10] In La_2LiMoO_6, the distances range from 2.099 to 2.155, with O−Li−O angles near 90°.[11] Distorted LiO_4 tetrahedra with bonds from 2.01 to 2.18 Å are observed in $Li_2La_{0.833}Nb_{1.5}Ti_{0.5}O_7$.[12] In $LiAl(P_2O_6)_2$ lithium occupies very distorted tetrahedra, with O−Li−O angles ranging from 77° to 130° and bond lengths ranging from 1.88 to 2.06 Å.[12] In sulfides, distorted tetrahedral coordination (angles 104−125°) is observed in Li_4GeS_4.[13]

The T2 structure contains 12 formula units of $Li_{2/3}MO_2$ in the orthorhombic unit cell (*Cmca*). There are 24 possible distorted tetrahedral sites: 8e (1/4, *y*, 1/4) and 16g (*x*, *y*, *z*). Since 8e has a higher symmetry, we chose 8e as filled and 16g as empty, which gives the correct stoichiometry, $x = 2/3$, in $Li_x[Ni_{1/3}Mn_{2/3}]O_2$.

Confirmation of the Transition-Metal Ordering in T2−$Li_{2/3}[Ni_{1/3}Mn_{2/3}]O_2$ by Neutron Diffraction. The proposed transition-metal ordering in T2-$Li_{2/3}[Ni_{1/3}Mn_{2/3}]O_2$, as well as the positions of the lithium atoms, had to be confirmed by neutron diffraction. Neutron diffraction is very sensitive to Ni−Mn ordering since Mn and Ni have very different scattering lengths. In addition, lithium is a strong neutron scatterer. In the $(\sqrt{3})a$ by $(\sqrt{3})a$ superstructure, the nickel atoms are thought to occupy the sites as indicated in Figure 3, which we call A_1 here. The Mn atoms occupy A_2 and A_3 sites. Each of the A_1, A_2, and A_3 sites lie on the A sites of the small hexagonal cell as shown in the figure. In the P2 structure, the metal atoms align on A sites as the layers are stacked (Figure 2). Neutron scattering can determine the stacking sequence of the Ni atoms in adjacent layers, i.e., $A_1A_1A_1A_1$... or $A_2A_3A_2A_3$... .

Figure 10 shows the neutron diffraction pattern of the crystalline $Li_{2/3}[Ni_{1/3}Mn_{2/3}]O_2$ sample LiNi1, together with a calculated pattern using the refined crystal data given in Table 4. Note that a perfect refinement is not possible, caused by the irregularities of the experimental pattern. The crystal data are almost the same as those proposed earlier from the X-ray diffraction analysis (Table 3). To achieve a satisfactory agreement between the calculated and observed neutron patterns, especially at large angles, it was necessary to refine the oxygen positions. In the X-ray refinement, oxygen was fixed at the "hexagonal sites" (0, 1/3, *z*) and (1/3, 1/3, *z*). A significant deviation of the oxygen positions from the hexagonal sites would cause superstructure peaks that were not observed. However, the obtained corrections are sufficiently small. Recalculating the X-ray spectrum using the oxygen positions obtained by the neutron diffraction−Rietveld refinement yields intensities of less than 0.5% for superstructure peaks at scattering angles of 20.8°, 22.7°, 27.4°, and 34.0°. In fact, the calculated peaks coincide with some of the "noise" observed in Figure 5b. The refinement for sample LiNi1 yields a fraction of only 10% Mn on Ni sites and only 5% Ni on Mn sites. The neutron data perfectly support the *novel* T2 structure proposed from the X-ray analysis. Note that the Ni and Mn cation ordering can be described by a face-centered orthorhombic unit cell (see Figure 8).

Table 4. Crystal Data of T2-$Li_{2/3}[Ni_{1/3}Mn_{2/3}]O_2$ Obtained from Neutron Diffraction of the Crystalline Sample LiNi1

T2-$Li_{2/3}[Ni_{1/3}Mn_{2/3}]O_2$[a] space group *Cmca*, orthorhombic				
$N = 4$	*x*	*y*	*z*	occ
Ni	0	0	0	0.89
Mn	0	0	0	0.11
Ni	1/3	0	0	0.11
Mn	1/3	0	0	1.89
O(1)	0	0.355	0.103	2
O(2)	0.321	0.327	0.109	4
Li	1/4	0.096	1/4	1.60

[a] $R_B = 4.3\%$, $A_{orth} = 8.614$ Å, $B_{orth} = 4.959$ Å, $C_{orth} = 10.069$ Å.

Structure of O6-$Li_{2/3}[Mg_{1/3}Mn_{2/3}]O_2$. The magnesium-containing $Li_{2/3}[Mg_{1/3}Mn_{2/3}]O_2$ could show cation ordering similar to that of nickel-containing T2-$Na_{2/3}[Ni_{1/3}Mn_{2/3}]O_2$. Presumably both nickel and magnesium are divalent in these compounds and fit rather well in the MnO_2 layers. The cation ordering in $Li_{2/3}[Mg_{1/3}Mn_{2/3}]O_2$ can be investigated by X-ray diffraction since the scattering powers of Mg and Mn are sufficiently different.

Figure 11 shows the X-ray diffraction pattern of $Li_{2/3}[Mg_{0.3}Mn_{0.7}]O_2$. [The X-ray pattern of $Li_{2/3}[Mg_{0.25}Mn_{0.75}]O_2$ is almost identical.] Since only a tiny peak at 16° remains from the initial sodium bronze, the ion exchange has almost been completed. The Bragg peaks have been indexed using the base of the small hexagonal unit cell and a *c* axis corresponding to six MO_2 layers. All peaks, except one small peak at 17.9° and a shoulder at 78.6°, could be indexed using this cell. Table 5 gives a comparison between observed and calculated Bragg positions using this unit cell. We believe that the basic structure is the O6 structure as shown in Figure 12. The (1/3, 1/3, *l*) peaks between 20° and 35° give clear evidence for the Mg−Mn ordering on the $(\sqrt{3})a$ by $(\sqrt{3})a$ superlattice.

Figure 11 also shows a calculated pattern based on the O6 structure at the bottom. Since we could not find a hexagonal or rhombohedral space group compatible with a six-layer unit cell that allows the $(\sqrt{3})a$ by $(\sqrt{3})$-

(10) Cormier, L.; Gaskell, P. H.; Calas, G.; Zhao, J.; Soper, A. K. *Phys. Rev. B* **1998**, *57*, R8068.
(11) Tortelier, J.; Gougeon, P. *Acta Crystallogr. C* **1996**, 500.
(12) Crosnier-Lopez, M. P.; Bhuvanesh, N. S. P.; Duroy, H.; Fourquet, J. L. *J. Solid State Chem.* **1999**, *145*, 136.
(13) Matsushita, Y.; Kanatzidis, M. G.; *Z. Naturforsch.* **1998**, *53B*, 23−30.

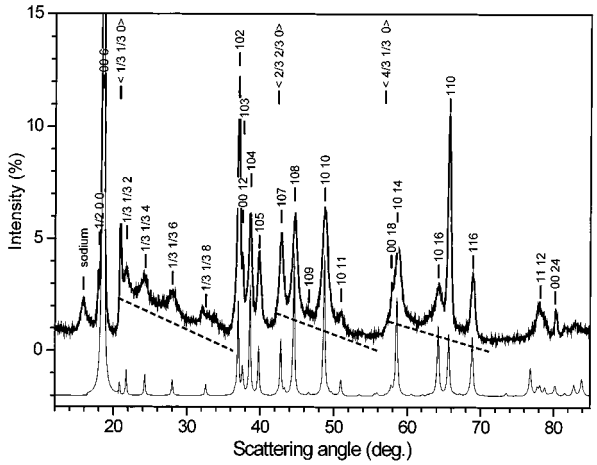

Figure 11. X-ray diffraction pattern of O6-type $Li_{2/3}[Mg_{0.3}Mn_{0.7}]O_2$. Miller indices are given for the small hexagonal unit cell. Thick line: observed spectrum. Thin line: calculated spectrum for O6-$Li_{2/3}[Mg_{0.3}Mn_7]O_2$ without stacking faults.

Table 5. Observed and Calculated Peak Positions for O6-$Na_{2/3}[Mg_{1/3}Mn_{2/3}]O_2$[a]

h	*k*	*l*	2θ obsd	2θ correctd	2θ calcd	diff
			17.877	17.861		
0	0	6	18.549	18.533	18.55	−0.017
1/3	1/3	0	20.898*	20.881	20.82	0.061
1/3	1/3	2	21.668*	21.652	21.732	−0.080
1/3	1/3	4	24.033*	24.016	24.271	−0.255
1/3	1/3	6	27.88*	27.64	28.025	−0.161
1/3	1/3	8	32.546*	323	32.613	0.082
1	0	2	37.045	37.029	37.029	0.000
0	0	12	37.641	37.625	37.61	0.015
1	0	4	38.619	38.603	38.647	−0.044
1	0	5	39.863	39.848	39.824	0.024
1	0	7	42.856	42.841	42.829	0.011
1	0	8	44.689	44.673	44.624	0.049
1	0	9	46.546	46.531	46.591	−0.060
1	0	10	48.763	48.748	48.717	0.031
1	0	11	51.007	50.992	50.989	0.003
0	0	18	57.846	57.831	57.832	−0.001
1	0	14	58.669	58.654	58.585	0.069
1	0	16	64.161	64.147	64.238	−0.091
1	1	0	65.66	65.646	65.651	−0.004
1	1	6	68.899	68.885	68.879	0.006
1	1	12	77.918*	77.904	78.201	−0.297
			78.625*	78.612	84.376	
0	0	24	80.309	80.297	80.287	0.010

[a] Hexagonal, $a_{hex} = 2.844$ Å, $c_{hex} = 28.698$ Å. Observed peaks were corrected for an off-axis shift of 29 μm. Observed peak positions marked with an asterisk were excluded in the refinement.

a superlattice, the monoclinic space group *C*12/*m*1 was used. Crystal data are given in Table 6. The features of the calculated spectrum match the features of the observed spectrum fairly well. The peak positions are correct, and the intensity ratios are approached. The only serious distinction is a strong (1, 0, 20) peak (76.82°), which is not observed experimentally. The broadening of the (1, 0, *l*) peaks is most likely caused by stacking faults. The lattice constants of the monoclinic cell were chosen so that the base of the monoclinic cell has no distortion (a_{mon}:b_{mon} = 1:$\sqrt{3}$) from the hexagonal cell. In addition, the monoclinic angle β and *c* axis were chosen so that there is no distortion from the hexagonal cell. [$a_{mon} = (\sqrt{3})a_{hex}$; $b_{mon} = 3a_{hex}$; $c_{mon} = (1/3)(3a^2_{hex} + c^2_{hex})^{1/2}$; $\beta = 180° - \text{atan}\{c_{hex}/((\sqrt{3})a_{hex})\}$.] The left part of Figure 12 displays the stacking in O6 using a monoclinic cell (dashed) and the hexagonal cell (solid). The right figure shows the monoclinic unit cell. The presented data prove that $Li_{2/3}[Mg_{0.3}Mn_{0.7}]O_2$ crystallizes in an O6-type structure. This is to our knowledge the first report of a material directly prepared in this structure. Until now O6 was only obtained from O2-type $LiCoO_2$ during chemical or electrochemical deintercalation of lithium.[2]

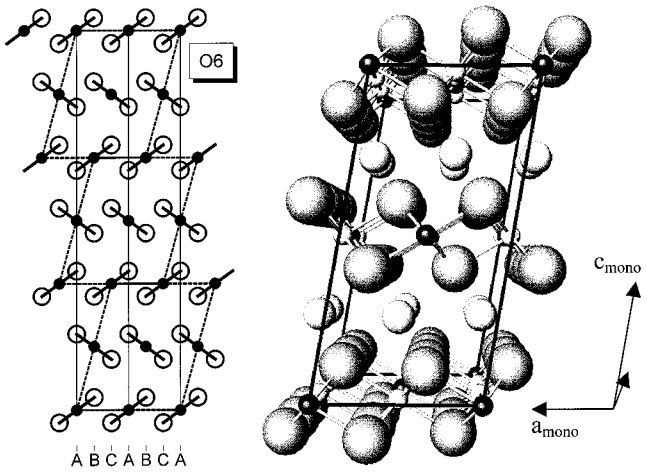

Figure 12. O6 structure. The figure displays the relation between the six-layer small hexagonal unit cell and the two-layer small monoclinic cell.

Table 6. Crystal Data Used in the Calculation of the X-ray Diffraction Pattern (Not Refined) of O6-$Li_{2/3}[Mg_{0.3}Mn_{0.7}]O_2$ and Crystal Data of P2-$Na_{2/3}[Mg_{0.25}Mn_{0.75}]O_2$ Obtained from the X-ray Diffraction of the Precursor NaMg2

O6-$Li_{2/3}[Mg_{0.3}Mn_{0.7}]O_2$[a] space group *C*12/*m*1, monoclinic					P2-$Na_{2/3}[Mg_{1/4}Mn_{3/4}]O_2$[b] space group *P*6$_3$/*mcm*, hexagonal				
N = 2	*x*	*y*	*z*	occ	*N* = 2	*x*	*y*	*z*	occ
$Mg_{0.9}Mn_{0.1}$	0	0	0	1	Mg	0	0	0	0.70
Mn	0	1/3	0	2	Mn	0	0	0	0.30
$Mg_{0.9}Mn_{0.1}$	0	0	0.5	1	Mg	1/3	2/3	0	0.05
Mn	0	1/3	0.5	2	Mn	1/3	2/3	0	1.95
O	0.4	0	0.08	2	O	0.354	0.354	0.08	6.26
O	0.4	2/3	0.08	4	Na	0.301	0	1/4	0.94
O	0.266	0	0.42	2	Na	0	0	1/4	−0.02
O	0.266	1/3	0.42	4	Na	1/3	2/3	1/4	0.70

[a] $A_{mon} = 4.926$ Å, $B_{mon} = 8.532$ Å, $C_{mon} = 9.706$ Å, $\beta = 99.74°$. [b] GOF = 2.0, $R_B = 4.0\%$, $A_{hex} = 5.009$ Å, $C_{hex} = 11.218$ Å.

Structure of the Precursor $Na_{2/3}[Ni_{1/3}Mn_{2/3}]O_2$. Figure 5a shows that precursor NaNi1, $Na_{2/3}[Ni_{1/3}Mn_{2/3}]O_2$, is single-phase hexagonal P2. Some of the very small impurities or peaks at scattering angles of 22.0°, 27.3°, and 28.4° could be caused by the Ni−Mn superstructure. Figure 13 shows the detailed X-ray pattern for precursor NaNi1 ($Na_{2/3}[Ni_{1/3}Mn_{2/3}]O_2$) after the K$\alpha_2$ component of the pattern was subtracted. Figure 13 also shows a calculated pattern based on Rietveld refinement that agrees well with experiment. The small hexagonal unit cell was used since the superstructure peaks are too weak to allow a better refinement using the large hexagonal unit cell. The initial $Na_{2/3}[Ni_{1/3}Mn_{2/3}]O_2$ precursor has the hexagonal P2 structure without an orthorhombic or a monoclinic distortion. This is interesting since we can assume that the precursor is ordered. [The ion-exchanged T2-$Li_{2/3}[Ni_{1/3}Mn_{2/3}]O_2$ exhibits Ni−Mn cation ordering. It is unlikely that this ordering was absent before ion exchange.] It shows that the ordering must be compatible with a two-layer hexagonal (or rhombohedral) space group. The crystal

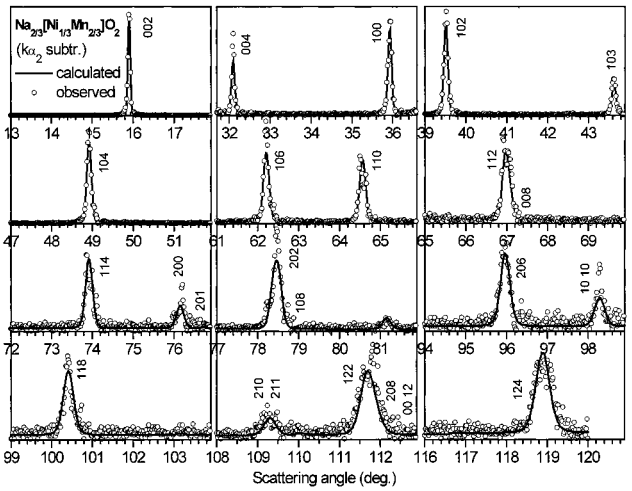

Figure 13. Observed X-ray diffraction pattern and Rietveld refinement of the highly crystalline precursor NaNi1 ($Na_{2/3}[Ni_{1/3}Mn_{2/3}]O_2$). Data are corrected for the $K\alpha_2$ radiation. The crystal data of the Rietveld refinement are given in Table 3. The spectrum can be perfectly indexed using the small hexagonal unit cell.

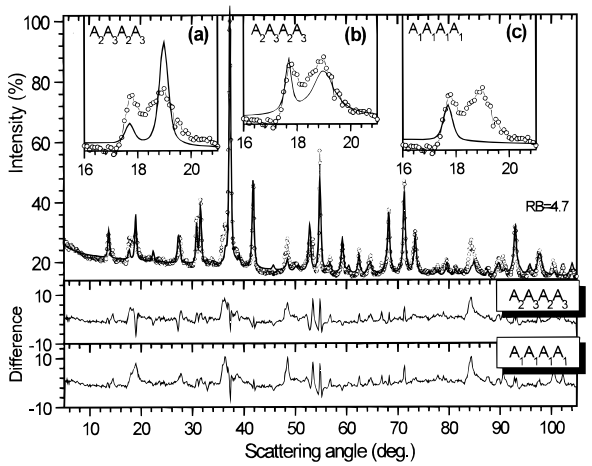

Figure 14. Neutron diffraction data and Rietveld refinement of $Na_{2/3}[Ni_{1/3}Mn_{2/3}]O_2$ (precursor P3). Two different stackings of the $(\sqrt{3})a \times (\sqrt{3})a$ a ordered $Ni_{1/3}Mn_{2/3}O_2$ layers were tried, either $A_1A_1A_1A_1$... or $A_2A_3A_2A_3$... . The Bragg R factor (R_B) is similar. The insets display the refinement for the superstructure peaks (1/3, 1/3, 0) and (1/3, 1/3, 1). Inset a: refinement for the (1/3, 1/3, 0) and (1/3, 1/3, 1) peaks using the $A_2A_3A_2A_3$... stacking sequence. Inset b: same as inset A but with peak widths adjusted while keeping the integrated intensities the same. Inset c: refinement for the (1/3, 1/3, 0) and (1/3, 1/3, 1) peaks using the $A_1A_1A_1A_1$... stacking sequence.

data obtained by the Rietveld refinement are given in Table 3.

Neutron diffraction is required to investigate the cation ordering in the P2 precursors. Unfortunately, we have no diffraction data for the crystalline precursor. We show here data for a less crystalline material, precursor "P3" described in ref 9. [The X-ray diffraction pattern of precursor P3 is similar but less crystalline than that of the crystalline precursor NaNi1. Precursor P3 could be ion-exchanged, leading to a sample which is the T2 structure.[9]] Figure 14 shows the observed neutron spectrum of $Na_{2/3}[Ni_{1/3}Mn_{2/3}]O_2$ precursor P3 together with the results of the Rietveld refinement. The insets of the figure show that the refinement using the $A_2A_3A_2A_3$ stacking (insets a and b) matches the superstructure peaks much better than the refinement using the $A_1A_1A_1A_1$... stacking (inset c). In the calculated pattern due to $A_1A_1A_1A_1$ stacking, the peaks (1/3, 1/3, 1) and (4/3, 1/3, 1) are completely absent, while they are observed in the experiment. The $A_2A_3A_2A_3$ stacking gives the correct integrated intensities for (1/3, 1/3, 0) and (1/3, 1/3, 1) and gives some intensity for (4/3, 1/3, 1). Some major differences between the observed and calculated patterns can be attributed to nonuniform peak width. Inset a enlarges the region of superstructure peaks. The peak shapes are peculiar and probably indicate stacking faults. The refinement cannot fit this region correctly. Inset b redisplays the observed pattern together with a calculated pattern where the peak widths, not integrated intensities, of the (1/3, 1/3, 0) and (1/3, 1/3, 1) peaks have been adjusted to match the data. There is good agreement. Furthermore, the $A_2A_3A_2A_3$ refinement suggests that the Ni−Mn ordering in the layers is not perfect. It yields 0.7 Ni and 0.3 Mn on nickel sites and 0.15 Ni and 0.85 Mn on manganese sites. We conclude that $Na_{2/3}[Ni_{1/3}Mn_{2/3}]O_2$ has the P2 structure with a predominantly $A_2A_3A_2A_3$ stacking sequence of (partially) superstructure-ordered MO_2 sheets.

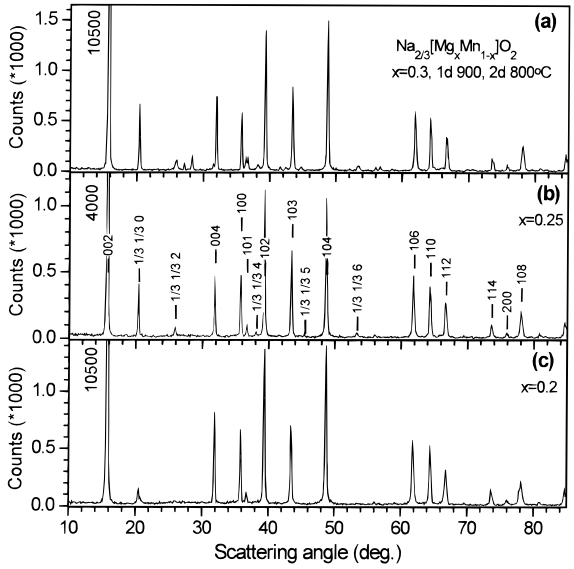

Figure 15.

Structure of the Precursor $Na_{2/3}[Mg_{1/3}Mn_{2/3}]O_2$. T2-$Li_{2/3}[Ni_{1/3}Mn_{2/3}]O_2$ was obtained from a precursor P2-$Li_{2/3}[Ni_{1/3}Mn_{2/3}]O_2$ which had the $A_2A_3A_2A_3$ type of cation ordering. It would be interesting to understand whether the P2-type $Na_{2/3}[Mg_{1/3}Mn_{2/3}]O_2$ precursor has a different cation ordering that leads to the alternative O6 structure observed for $Li_{2/3}[Mg_{1/3}Mn_{2/3}]O_2$ after ion exchange.

The precursors tempered at 800 °C showed clear evidence of cation ordering. Figure 15 shows the X-ray diffraction pattern of the three $Na_{2/3}[Mg_xMn_{1-x}]O_2$ precursors ($x = 0.2$, $x = 0.25$, and $x = 0.3$) which were prepared at 900 °C (1 day) and tempered at 800 °C (2 days). All precursors have the P2 structure. The patterns are indexed using the small hexagonal cell. Clearly a series of (1/3, 1/3, l) superstructure peaks evolves as x approaches 1/3, suggesting a $(\sqrt{3})a$ a by $(\sqrt{3})a$ Mg−Mn superstructure in the sheets. [Samples tempered at 1000 °C and quenched do not show superstructure

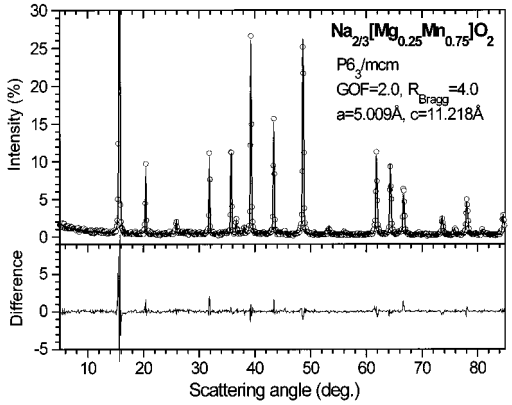

Figure 16. X-ray diffraction pattern and Rietveld refinement of the P2-type $Na_{2/3}[Mg_xMn_{1-x}]O_2$, $x = 0.25$. Crystal data are given in Table 6.

peaks. Therefore, an order−disorder phase transformation probably occurs above 900 °C. The sample with $x = 1/3$ (not single-phase material) showed a different Mg−Mn-ordered stacking (probably $A_2A_3A_2A_3$, since the (1/3, 1/3, 1) peak exists). It had a less crystalline spectrum with variable peak widths.] Figure 16 shows the X-ray diffraction pattern of $Na_{2/3}[Mg_xMn_{1-x}]O_2$ with $x = 0.25$. The pattern could be perfectly refined assuming an $A_1A_1A_1A_1$ stacking sequence. The crystallographic data are given in Table 6. In the refinement only the Mg:Mn ratio was fixed, and no vacancies on transition-metal sites were allowed. The obtained occupation numbers agree with the assumed stoichiometry of $Na_{2/3}MO_2$. Note that the sodium sites on A_1 (of the large hexagonal cell) are empty. Clearly the $A_1A_1A_1A_1$ stacking of ordered $Mg_xMn_{1-x}O_2$ sheets induces an ordering of sodium which is not observed for the other P2 phases. The pattern has peaks whose widths change smoothly with the angle. Therefore, we can conclude that the ordered $Mg_xMn_{1-x}O_2$ sheets are stacked without severe stacking faults.

P2-$Na_{2/3}[Ni_{1/3}Ti_{2/3}]O_2$ and O2-Type $Li_{2/3}[Ni_{1/3}Ti_{2/3}]O_2$. We tried to prepare the precursor-phase $Na_{2/3}[Ni_{1/3}Ti_{2/3}]O_2$ and $Li_{2/3}[Ni_{1/3}Ti_{2/3}]O_2$ by ion exchange. This phase is isovalent to the $M = Ni_{1/3}Mn_{2/3}$ and $M = Mg_{1/3}Mn_{2/3}$ phases. Figure 17a shows the X-ray diffraction pattern of P2-$Na_{2/3}[Ni_{1/3}Ti_{2/3}]O_2$ together with a refined pattern using the hexagonal P2 structure. Figure 17b gives the difference of the refined and observed patterns. To our knowledge a P2-sodium bronze predominantly containing titanium has not been reported before. Ti and Ni have slightly different scattering powers, so in the case of a strong $(\sqrt{3})a$ by $(\sqrt{3})a$ Ni−Ti ordering, superstructure peaks should be visible. We expect the intensity to be about 0.5% of that of the main (002) peak. No peaks are detectable above the noise as the inset (Figure 17d) shows. This absence indicates the absence of a strong Ni−Ti ordering, although neutron scattering would give better proof.

Figure 17c gives the X-ray diffraction pattern of $Li_{2/3}[Ni_{1/3}Ti_{2/3}]O_2$ after ion exchange in aqueous LiOH solution at room temperature. The ion exchange has been completed. It shows a structure that we have been unable to index convincingly apart from the (002), (110), and (112) peaks of the small hexagonal cell. It is not the orthorhombic T2 structure since the (111) peak is missing, but we believe it to have an O2-type structure.

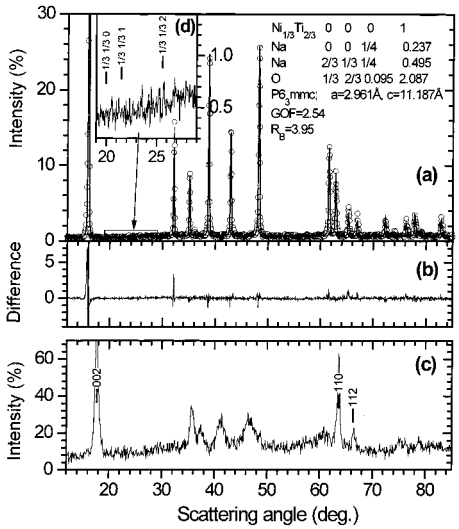

Figure 17. X-ray diffraction pattern and Rietveld refinement of P2-$Na_{2/3}MO_2$ and O2-type $Li_{2/3}MO_2$ (M = $Ni_{1/3}Ti_{2/3}$). (a) Observed and calculated spectrum for P2-$Na_{2/3}MO_2$. Crystal data are given in the figure. (b) Difference between the observed and calculated patterns. (c) X-ray diffraction pattern of O2-$Li_{2/3}[Ni_{1/3}Ti_{2/3}]O_2$ prepared by ion exchange in H_2O. (d) The inset shows the absence of $(\sqrt{3})a \times (\sqrt{3})a$ superstructure peaks.

Several further attempts to prepare layered P2-bronzes $Na_{2/3}[A^{II}{}_{1/3}B^{IV}{}_{2/3}]O_2$ from A = Mg, Zn, Ni, Fe and B = Mn, Ti were unsuccessful. However, it is likely that more isostoichiometric sodium bronzes exist. If potassium were included in the initial P2 phase, we expect other compositions could be stabilized. For example, its larger size might allow larger cations (Zr^{IV}, Sn^{IV}, etc.) in the MO_2 layers. As an example, P2-$K_{2/3}[Mg_{1/3}Sn_{2/3}]O_2$ (which is isovalent to $Na_{2/3}[Ni_{1/3}Mn_{2/3}]O_2$) has been reported.[5]

Discussion

It shall be argued that the stability of the orthorhombic T2 structure (compared with the O2 structure) of $Li_{2/3}[Ni_{1/3}Mn_{2/3}]O_2$ is related to the existence of the $(\sqrt{3})a$ by $(\sqrt{3})a$ Ni−Mn superstructure within the MO_2 layers. Assume as starting sodium bronze a P2-$Na_{2/3}MO_2$ without transition-metal ordering. The space group is $P6_3/mmc$. Since lithium does not accept prismatic sites, the MO_2 layers glide during ion exchange to make octahedral sites. This results in the O2 (or alternatively in the O6) structure. In both cases the crystallographic lithium sites are 2/3 filled. A statistical 2/3 filling of all sites in one layer seems unsatisfying, and an ordering appears favored. However, no hexagonal or rhombohedral space group allows the general stacking of the O2 or O6 structure and, simultaneously, delivers a $(\sqrt{3})a$ by $(\sqrt{3})a$ superstructure for the lithium atoms. This general consideration correlates with the fact that the direct preparation of crystalline O2−Li_xMO_2 with $x = 2/3$ appears to be difficult. As an example, $Na_{2/3}MnO_2$ yields poorly crystalline O2-$Li_{2/3}MnO_2$ after ion exchange with severe stacking faults.[14] [A crystalline O2 structure was achieved for Li_xCoO_2. However, here the stoichiometry is $x = 1$. After extraction of lithium to x

(14) Paulsen, J. M.; Dahn, J. R. *Solid State Ionics* **1999**, *126*, 3−24.

$\cong$ 2/3 a strong (111) peak evolves.[15] This peak is forbidden in ideal O2, indicating that a T2-type structure may have evolved.]

Now assume that the initial sodium bronze is P2-$Na_{2/3}[M'_{1/3}Mn_{2/3}]O_2$, having a $(\sqrt{3})a$ by $(\sqrt{3})a$ superstructure within the MO_2 layers. In the P2 structure all the transition metals are located on the A sites of the small hexagonal cell. To describe the transition-metal ordering, the large hexagonal cell is required. Here the transition-metal atoms are located on the A_1, A_2, and A_3 sites. Two different stackings of the $(\sqrt{3})a$ by $(\sqrt{3})a$ superstructures in the M′ and M atoms are compatible with a two-layer hexagonal cell. The space group $P6_3/mcm$ yields a stacking where all M′ atoms are located on top of M′ atoms and Mn on top of Mn. This stacking is the $A_1A_1A_1A_1$ stacking. We observed it for $Na_{2/3}[Mg_{0.25}Mn_{0.75}]O_2$ and $Na_{2/3}[Mg_{0.3}Mn_{0.7}]O_2$ tempered at 800 °C. The space group $P6_3$ yields a structure where the M′ atoms are stacked differently. If M′ is on an A_2 site in one layer, then the M′ of the next layer is on an A_3 site. This stacking is the $A_2A_3A_2A_3$... stacking. This stacking was observed for $Na_{2/3}[Ni_{1/3}Mn_{2/3}]O_2$.

During ion exchange the layers glide since lithium does not accept prismatic sites. However, any gliding destroys the hexagonal or rhombohedral symmetry of the large unit cell. Therefore, no large hexagonal unit cell can describe $Li_{2/3}[M'_{1/3}Mn_{2/3}]O_2$ with transition-metal ordering. Instead, a large orthorhombic or large monoclinic unit cell is required. Fortunately, nature often chooses the highest possible symmetry. The most symmetric structures which yield the alternating orientation of the MO_2 sheets and simultaneously yield a $(\sqrt{3})a$ by $(\sqrt{3})a$ superstructure within the MO_2 sheets are the P2 and T2 structures. The P2 structure has prismatic sites, which are not accepted by lithium. Therefore, the T2 structure has the highest possible symmetry which can be achieved for $Li_{2/3}[M'_{1/3}Mn_{2/3}]O_2$.

Let us assume that a layer gliding by more than one lattice position (of the small hexagonal cell) is impossible. If the layer, for example, has to glide 1.5 lattice sites, then it will cross a configuration after gliding 0.5 lattice sites that is very similar to the final one. It would be identical if transition-metal ordering were neglected. If the final structure (after gliding 1.5 sites) is energetically preferred, then the intermediate configuration will also exhibit a pronounced stability. Therefore, the gliding will stop there. A closer examination shows that the orthorhombic T2 structure only can be achieved if the transition-metal ordering of the initial P2-$Na_{2/3}[M'_{1/3}Mn_{2/3}]O_2$ is $A_2A_3A_2A_3$. Otherwise, the M′ atoms in the gliding layer cannot move to the required place with a glide of less than one small hexagonal lattice constant. Therefore, the T2 structure results after ion exchange for $Na_{2/3}[Ni_xMn_{1-x}]O_2$, which has the $A_2A_3A_2A_3$ ordering, but not for $Na_{2/3}[Mg_xMn_{1-x}]O_2$, which has the $A_1A_1A_1A_1$ ordering. In the latter case the highest symmetry is monoclinic, and in fact, a monoclinic space group is observed.

Further observations confirm the close relationship between the 2/3 alkali:1/3 M′:2/3 M stoichiometry, the cation ordering within the MO_2 sheets, and the final T2 structure. The more the stoichiometry of $Na_{2/3}[Ni_xMn_{1-x}]O_2$ deviates from $x = 1/3$, the more the ion-exchanged $Li_{2/3}[Ni_xMn_{1-x}]O_2$ approaches the stacking-faulted O2 structure instead of the crystalline T2 structure.[9]

Summary

Layered compounds $A_{2/3}[M'^{2+}{}_{1/3}M^{4+}{}_{2/3}]O_2$ have been studied for A = Li, Na, M′ = Ni, Mg, and M = Mn, Ti. The metastable compounds with A = Li were uniformly prepared from P2 structure precursors with A = Na by ion exchange. We showed that when M′ = Ni and Mg and M = Mn, the transition-metal layers are ordered on a $(\sqrt{3})a$ by $(\sqrt{3})a$ superlattice that is preserved during ion exchange. When M = Ti, no evidence for transition-metal ordering was observed.

Using the results from X-ray and neutron scattering, $Li_{2/3}[Ni_{1/3}Mn_{2/3}]O_2$ was shown to adopt a new orthorhombic structure that we call T2. In the notation of Hagenmuller and Delmas, the T2 structure has a two-layer unit cell and tetrahedral sites for lithium. $Li_{2/3}[Mg_{1/3}Mn_{2/3}]O_2$ adopts an O6 structure, and $Li_{2/3}[Ni_{1/3}Ti_{2/3}]O_2$ probably adopts an O2-type structure. We focused on the novel T2 structure and gave arguments for its formation based on the stacking of the ordered transition-metal layers.

The electrochemical properties of these and other new phases based on O2, O6, and T2 structures need to be measured as these materials could be of great importance as cathodes for rechargeable Li ion batteries.

Acknowledgment. We acknowledge the support of 3M Co., 3M Canada Co., NSERC, and NRC for the funding of this work.

CM990810D

(15) Paulsen, J. M.; Mueller-Neuhaus, J. R.; Dahn, J. R. *J. Electrochem. Soc.* **1999**, *147*, 508.